

## Discrepant Effects of Atmospheric Adjustments in Shaping the Spatial Pattern of SST Anomalies between Extreme and Moderate El Niños

JUN YING,<sup>a,b,c</sup> TAO LIAN,<sup>a,d,c</sup> PING HUANG,<sup>e,b</sup> GANG HUANG,<sup>b,f</sup> DAKE CHEN,<sup>a,d,c</sup> AND SHANGFENG CHEN<sup>e</sup>

<sup>a</sup> State Key Laboratory of Satellite Ocean Environment Dynamics, Second Institute of Oceanography, Ministry of Natural Resources, Hangzhou, China

<sup>b</sup> State Key Laboratory of Numerical Modeling for Atmospheric Sciences and Geophysical Fluid Dynamics, Institute of Atmospheric Physics, Chinese Academy of Sciences, Beijing, China

<sup>c</sup> Southern Marine Science and Engineering Guangdong Laboratory (Zhuhai), Zhuhai, China

<sup>d</sup> School of Oceanography, Shanghai Jiao Tong University, Shanghai, China

<sup>e</sup> Center for Monsoon System Research, Institute of Atmospheric Physics, Chinese Academy of Sciences, Beijing, China

<sup>f</sup> University of Chinese Academy of Sciences, Beijing, China

(Manuscript received 28 September 2020, in final form 19 March 2021)

**ABSTRACT:** The surface heat flux anomalies during El Niño events have always been treated as an atmospheric response to sea surface temperature anomalies (SSTAs). However, whether they play roles in the formation of SSTAs remains unclear. In this study, we find that the surface net heat flux anomalies in different El Niño types have different effects on the development of the spatial pattern of SSTAs. By applying the fuzzy clustering method, El Niño events during 1982–2018 are classified into two types: 1) extreme El Niños with strong positive SSTAs, with the largest SSTAs in the eastern equatorial Pacific, and 2) moderate El Niños with moderate positive SSTAs, with the largest SSTAs in the central equatorial Pacific. The surface net heat flux anomalies in extreme El Niños generally display a “larger warming gets more damping” zonal paradigm, and essentially do not impact the formation of the spatial pattern of SSTAs. Those in moderate El Niños, however, can impact the formation of the spatial pattern of SSTAs by producing more damping effects in the eastern than in the central equatorial Pacific, thus favoring the largest SSTAs being confined to the central equatorial Pacific. More damping effects of net heat flux anomalies in the eastern equatorial Pacific in moderate El Niños are contributed by the surface latent heat flux anomalies, which are mainly regulated by the negative relative humidity–SST feedback and the positive wind–evaporation–SST feedback. Therefore, we highlight that these two atmospheric adjustments should be considered during the development of moderate El Niños in order to obtain a comprehensive understanding of the formation of El Niño diversity.

**KEYWORDS:** ENSO; Climate change; Climate variability; El Niño

### 1. Introduction

El Niño events are characterized by anomalous warm sea surface temperature (SST) in the central-eastern equatorial Pacific, which have severe impacts on global climate and human society (Barsugli et al. 1999; Wu et al. 2004; McPhaden et al. 2006; Cai et al. 2015; Timmermann et al. 2018; Wei et al. 2020). In recent decades, extensive studies have revealed that El Niño events differ in terms of temporal evolution (Lengaigne and Vecchi 2010; Xie et al. 2018), amplitude (Chen et al. 2016; Cai et al. 2017), and spatial pattern (Ashok et al. 2007; Kao and Yu 2009; Kug et al. 2009; Chen et al. 2015). These differences give El Niño its different “flavors” and lead to different climate impacts (Alexander et al. 2002; An et al. 2007; Kim et al. 2009; Yuan and Yang 2012). In particular, the different spatial patterns of El Niño, generally measured by the different zonal locations of the largest SST anomalies (SSTAs), can induce distinct climate anomalies worldwide through air–sea interaction processes and atmospheric teleconnections (Horel and Wallace 1981; Larkin and Harrison 2005; Taschetto and England 2009; Taschetto et al. 2016; Xu et al. 2019). Understanding the diversity of spatial pattern of El Niño and its formation mechanisms are crucial for a reliable prediction of El Niño, as well as

the associated climate and socioeconomic impacts (Capotondi et al. 2015; Yang and Huang 2021).

One notable manifestation of the diversity of spatial pattern of El Niño is that most El Niño events present moderately warm SSTAs with the largest magnitude in the central Pacific, while a few extreme El Niños have extraordinarily warm SSTAs that are centered in the equatorial eastern Pacific close to the South American coast (Takahashi et al. 2011). Much attention has been paid to the differences in the formation mechanisms between extreme and moderate El Niños (Jin et al. 2003; Chen et al. 2015; Chen et al. 2016). For instance, oceanic nonlinear dynamic heating was revealed to be an essential role for developing extreme El Niños (Jin et al. 2003); oceanic vertical advection anomalies caused by thermocline deepening are believed to be the dominant contributor for extreme El Niños, but not for moderate ones (Kug et al. 2009; Chen et al. 2015); and zonal advection anomalies caused by anomalous zonal currents appear to be the most important factor contributing to the discrepant magnitudes of SSTAs in the eastern Pacific between extreme and nonextreme El Niños (Chen et al. 2016). However, these studies mainly concentrated on the role of dynamic ocean heat transport, with little attention on the discrepant effects of atmospheric adjustments on the development of SSTAs between extreme and moderate El Niños.

Corresponding author: Jun Ying, yingjun@sio.org.cn

DOI: 10.1175/JCLI-D-20-0757.1

© 2021 American Meteorological Society. For information regarding reuse of this content and general copyright information, consult the AMS Copyright Policy ([www.ametsoc.org/PUBSReuseLicenses](http://www.ametsoc.org/PUBSReuseLicenses)).

Brought to you by Institute of Atmospheric Physics, CAS | Unauthenticated | Downloaded 01/05/22 08:36 AM UTC

In general, atmospheric adjustments during the development of El Niño SSTAs are always treated as damping roles to balance the positive effects from dynamic ocean heat transport anomalies, as they produce negative surface heat flux anomalies (Jin et al. 2006; Zhang and McPhaden 2008; Chen et al. 2015; Chen et al. 2016; Lian et al. 2017). However, it has been revealed that the spatial patterns of surface heat flux anomalies do not always exhibit a straightforward reversed relationship with the pattern of SSTAs (Wang and McPhaden 2000; Pavlakis et al. 2008). For example, the surface latent heat flux anomalies near and to the west of the date line were revealed to play a positive role in the development of locally warm SSTAs owing to reduced surface wind speed (Wang and McPhaden 2000), and the largest negative shortwave radiation anomalies during El Niño events are usually found to be located to the west of the positive SSTA center as a result of more convective activities locally (Pavlakis et al. 2008; Pinker et al. 2017). These findings imply that atmospheric adjustments may not only act in damping roles, but could also impact the spatial pattern of El Niño SSTAs.

There are considerable differences in the atmospheric responses to warm SSTAs between extreme and moderate El Niños. For example, the intertropical convergence zone, whose climatological position is north of the equator, migrates toward the eastern equatorial Pacific and turns the normally dry cold tongue condition into heavy rainfall under an extreme El Niño, but maintains north of the equator under a moderate El Niño and keeps the rainfall anomalies in the eastern equatorial Pacific small (Cai et al. 2014, 2017; Hu and Fedorov 2018); also, the westerly anomalies induced by convective heating intrude into the eastern Pacific during an extreme El Niño, but are confined to the central-western Pacific during a moderate one (Lengaigne and Vecchi 2010; Xie et al. 2018; Peng et al. 2020). These different responses imply discrepant atmospheric adjustments between extreme and moderate El Niños, which may in turn lead to discrepant effects on the further development of SSTAs through coupled ocean–atmosphere interaction processes (Bjerknes 1969; Xie and Philander 1994). However, it is still unclear whether atmospheric adjustments play different roles in the developing phase of SSTAs between extreme and moderate El Niños. Moreover, whether atmospheric adjustments impact the formation of the spatial pattern of El Niño SSTAs, rather than merely acting in damping roles, also needs to be further explored.

In this study, we investigate the discrepant effects of atmospheric adjustments on the spatial pattern formations of SSTAs during the developing phase of extreme and moderate El Niños, as well as the underlying mechanisms. We find that surface net heat flux anomalies in extreme El Niños, generally displaying a “larger warming gets more damping” zonal paradigm, have little impact on the formation of the zonal pattern of SSTAs, while those in moderate El Niños can help shape the zonal pattern of SSTAs by producing more damping effects in the eastern than central equatorial Pacific, thus favoring larger SSTAs being located in the central equatorial Pacific.

The rest of the paper is organized as follows: section 2 describes the data and methods used in the study. Section 3 presents the main results, including the objective separation of

extreme El Niños from other moderate ones, the discrepant effects of surface net heat flux anomalies during the developing phase between extreme and moderate El Niños, and the associated formation mechanisms. Conclusions and discussion are given in section 4.

## 2. Data and methods

### a. Datasets

The monthly SST data are from the National Oceanic and Atmospheric Administration (NOAA) Optimum Interpolation SST, version 2, with a horizontal grid resolution of  $1^\circ \times 1^\circ$ , which is provided by the NOAA Earth Research Laboratory Physical Science Division (<http://www.esrl.noaa.gov/psd/data>). The monthly atmospheric data are from the fifth major global reanalysis developed by the European Centre for Medium-Range Weather Forecasts (ERA5; <https://cds.climate.copernicus.eu/cdsapp#!/dataset/reanalysis-era5-single-levels-monthly-means?tab=form>), with a horizontal resolution of  $0.25^\circ \times 0.25^\circ$ , including the surface latent heat flux, sensible heat flux, net shortwave radiation, net longwave radiation, precipitation, boundary layer height, surface zonal and meridional winds, surface wind speed, air temperature, and three-dimensional relative humidity. Besides, the monthly SST from ERA5 is chosen only for computing the regressions between SSTAs and relative humidity anomalies, and between SSTAs and boundary layer height anomalies. The monthly oceanic three-dimensional data are from the National Centers for Environmental Prediction (NCEP) Global Ocean Data Assimilation System (GODAS; <https://www.esrl.noaa.gov/psd/data/gridded/data.godas.html>), with a horizontal resolution of  $1/3^\circ$  longitude  $\times$   $1^\circ$  latitude. In addition, we also use surface net heat fluxes from GODAS and the NCEP–National Center for Atmospheric Research (NCAR) reanalysis (<https://psl.noaa.gov/data/gridded/data.ncep.reanalysis.html>) to confirm the results derived from ERA5. All the datasets are chosen for the period 1982–2018 during which all variables are available. The monthly anomalies are obtained by removing the long-term trend as well as the climatological annual cycle of the chosen time period, and then a 3-month running mean is applied to reduce the intraseasonal variability.

### b. Fuzzy clustering method

The fuzzy clustering method (FCM), which has been proved to be an effective pattern-classification technique in climate research (Kim et al. 2011; Chen et al. 2015), is used to classify different El Niño types in this study. Unlike some other El Niño classification techniques that rely on prior knowledge of different El Niño patterns (Kao and Yu 2009; Kug et al. 2009), the FCM does not need to presume the different patterns of El Niño ahead of time, while leaving the data to be self-clustering objectively (Feng et al. 2020). It is designed to group a set of given members into specified categories based on their degree of membership (DOM), which stands for the similarity of members to the centroids. The DOM is defined as the root-mean-squared Euclidean distance to the cluster center and can be expressed as

$$e^2 = \min \left[ \sum_{i=1}^M \sum_{j=1}^N P_{i,j}^2 (X_j - C_i)^2 \right], \quad (1)$$

where

$$P_{i,j} = a \times \left\{ \sum_{k=1}^M \left[ \frac{\|X_j - C_i\|^2}{\|X_j - C_k\|^2} \right]^2 \right\}^{-1} \quad (2)$$

and

$$C_i = \frac{\sum_{j=1}^N P_{i,j}^2 X_j}{\sum_{j=1}^N P_{i,j}^2}. \quad (3)$$

Here,  $N$  is the size of members,  $M$  is the number of cluster sets,  $X_j$  is the map of the member,  $C_i$  is the map of the  $i$ th cluster centroid,  $P_{i,j}$  is the DOM of  $X_j$  to  $C_i$ , the vertical bars ( $\| \cdot \|$ ) denote Euclidean distance, and  $a$  is a scale factor to guarantee that  $\sum_{i=1}^M P_{i,j} = 1$  for  $j = 1$  to  $N$ .

The members applied to the FCM here are a subset of the monthly SSTAs in the tropical Pacific (20°S–20°N, 150°E–90°W) during El Niño events. We first use a  $40^\circ \times 10^\circ$  window zonally sliding by  $2.5^\circ$  along the equator (5°S–5°N), starting from 150°E to 90°W, in order to obtain a set of regional mean SSTAs and the corresponding standard deviations (STDs). The month in which any regional-mean SSTA is greater than the corresponding positive STD and  $0.5^\circ\text{C}$  is then regarded as a warm record. When all the warm records are extracted, those segments with less than five successive months in the set of warm records are deleted. Moreover, as the peak time of El Niño tends to be phase locked in boreal winter (Tziperman et al. 1998), the warm segments that do not contain boreal wintertime (November–January) are also discarded. The remaining warm months are then used for our classification of different El Niño types. In addition, the type of a specific El Niño event is based on the type into which its DOM in boreal winter falls. Details regarding the application of the FCM technique in El Niño classification can also be found in Chen et al. (2015).

### c. Ocean mixed layer heat budget analysis

Following Ying et al. (2016), the mixed layer temperature tendency equation can be simplified as

$$C \frac{\partial T'_O}{\partial t} = Q'_u + Q'_v + Q'_w + Q'_{\text{net}} + Q'_{\text{res}}, \quad (4)$$

where the prime denotes the monthly anomaly;  $T'_O$  is the ocean mixed layer temperature anomaly;  $C = C_p \rho_o H$  is the heat capacity of the ocean mixed layer;  $C_p = 4000 \text{ J kg}^{-1}$  and  $\rho_o = 1025 \text{ kg m}^{-3}$  are the specific heat at constant pressure and density of seawater, respectively;  $H$  is the mixed layer depth, which is chosen as a constant of 30 m for simplicity, as in (Ying et al. 2016);  $Q'_u = C(u_o \partial T / \partial x)'$ ,  $Q'_v = C(v_o \partial T / \partial y)'$ , and  $Q'_w = C(w_o \partial T / \partial z)'$  are the ocean zonal, meridional, and vertical heat transport anomalies in the mixed layer, respectively;  $u_o$ ,  $v_o$ , and  $w_o$  are the ocean zonal, meridional, and

vertical current averaged in the mixed layer;  $Q'_{\text{net}}$  is the surface net heat flux anomalies (positive downward), including the anomalous surface latent heat flux ( $Q'_E$ ), sensible heat flux ( $Q'_H$ ), net longwave radiation ( $Q'_{\text{LW}}$ ), and net shortwave radiation ( $Q'_{\text{SW}}$ ); and  $Q'_{\text{res}}$  is the residual term, including anomalies in the ocean subgrid-scale processes such as vertical mixing and lateral entrainment (DiNezio et al. 2009; Ying et al. 2016).

### d. Decomposition of the surface latent heat flux anomaly

Among the surface heat fluxes, the latent heat flux plays a critical role in modulating SST variations (Wang and McPhaden 2000; Xie et al. 2010; Jia and Wu 2013), which can be calculated by the following bulk formula:

$$Q_E = \rho_a L C_E W q_s(T_s) (1 - \text{RH} e^{\alpha \Delta T}), \quad (5)$$

where  $\rho_a$  is surface air density,  $L$  is the latent heat of evaporation,  $C_E$  is the exchange coefficient,  $W$  is the surface wind speed at 10 m,  $q_s(T_s)$  is the saturated specific humidity,  $\text{RH}$  is the surface relative humidity,  $T_s$  is SST, and  $\Delta T = T_a - T_s$  is the difference between the surface air temperature ( $T_a$ ) and SST, denoting the surface stability; and  $\alpha = L / (R_v T_s^2) \approx 0.06 \text{ K}^{-1}$ , in which  $R_v$  is the ideal gas constant for water vapor. To estimate the contributions of each factor during the development of El Niño,  $Q'_E$  is decomposed following previous studies (Du and Xie 2008; Xie et al. 2010; Jia and Wu 2013) as shown:

$$Q'_E = \frac{\partial Q_E}{\partial T_s} T'_s + \frac{\partial Q_E}{\partial W} W' + \frac{\partial Q_E}{\partial \text{RH}} \text{RH}' + \frac{\partial Q_E}{\partial \Delta T} \Delta T'. \quad (6)$$

Each term on the right-hand-side of Eq. (6) can be expressed as follows:

$$Q'_{\text{EO}} = \frac{\partial Q_E}{\partial T_s} T'_s = \alpha \overline{Q_E} T'_s, \quad (7)$$

$$Q'_{\text{EW}} = \frac{\partial Q_E}{\partial W} W' = \frac{\overline{Q_E}}{W} W', \quad (8)$$

$$Q'_{\text{ERH}} = \frac{\partial Q_E}{\partial \text{RH}} \text{RH}' = \frac{-\overline{Q_E}}{e^{-\alpha \Delta T} - \text{RH}} \text{RH}', \quad (9)$$

$$Q'_{\text{EAT}} = \frac{\partial Q_E}{\partial \Delta T} \Delta T' = \frac{-\alpha \overline{Q_E} \text{RH}}{e^{-\alpha \Delta T} - \text{RH}} \Delta T'. \quad (10)$$

Here, an overbar and prime denote the monthly climatology and anomaly, respectively. Equation (7) represents the Newtonian cooling effect in response to SSTAs, while Eqs. (8)–(10) represent the atmospheric adjustments due to anomalies in surface wind speed, relative humidity, and surface stability, respectively. Specifically, the term  $Q'_{\text{EW}}$  is commonly known as the wind–evaporation–SST (WES) feedback (Xie and Philander 1994), which can be further decomposed into effects from surface zonal and meridional wind anomalies:

$$Q'_{\text{Eu}} = \frac{\overline{Q_E} \overline{u}}{W^2} u' \quad (11)$$

and

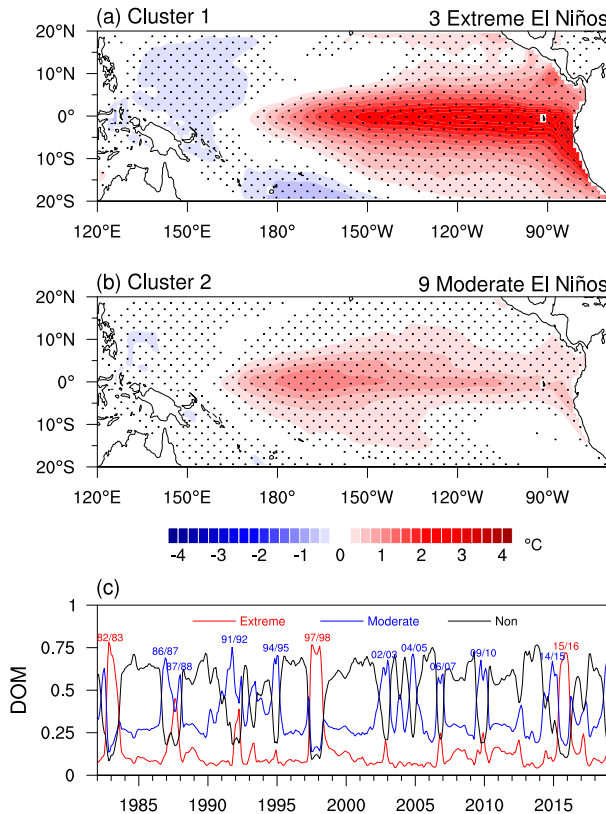


FIG. 1. The two El Niño clusters identified by the FCM and the associated DOMs: (a) the extreme El Niño cluster, which involves three historical extreme El Niño events; (b) the moderate extreme El Niño cluster, which includes nine historical moderate El Niño events; and (c) the DOM for extreme El Niño (red curve), moderate El Niño (blue curve), and neither (black curve). Stippling in (a) and (b) indicates that the compositions are significant at the 95% confidence level based on the Student's  $t$  test.

$$Q'_{Ev} = \frac{\overline{Q_E \bar{v}}}{W^2} v', \quad (12)$$

where  $u$  and  $v$  denote the surface zonal and meridional wind, respectively.

### 3. Results

#### a. Classification of El Niños based on the FCM

The FCM is applied to classify El Niño events during 1982–2018 into two types. As shown in Fig. 1, the first warm pattern displays robust positive SSTAs in the central and eastern Pacific and has its largest warming in the eastern equatorial Pacific near the South American coast (Fig. 1a), which is a typical feature of extreme El Niños (Takahashi et al. 2011; Chen et al. 2015; Xie et al. 2018). Three historical El Niños, commonly known as the extreme El Niño events of 1982/83, 1997/98, and 2015/16 (Cai et al. 2017; Lian et al. 2017), fall into the first pattern classification (Fig. 1c, red curve). The second warm pattern exhibits moderately positive SSTAs centered in

the central equatorial Pacific east of the date line around 170°W (Fig. 1b). Nine historical El Niños other than the three aforementioned extreme ones—in 1986/87, 1987/88, 1991/92, 1994/95, 2002/03, 2004/05, 2006/07, 2009/10, and 2014/15—are all classified as the second warm pattern (Fig. 1c, blue curve). Thus, the FCM naturally separates the extreme El Niños from other moderate El Niños when two clusters are set. Moreover, the classified result by the FCM indicates that the pattern differences between extreme and moderate El Niños appear to be the most robust among different El Niño types.

#### b. Discrepant roles of $Q'_{net}$ for the development of SSTA patterns between extreme and moderate El Niños

Figure 2 presents the spatial patterns of SSTAs, SSTA tendencies, and  $Q'_{net}$  during developing phase (from May to December of the developing year) of the extreme and moderate El Niños. It is shown that the largest SSTAs during the developing phase appear to be anchored basically in the eastern equatorial Pacific east of 150°W in extreme El Niños (Fig. 2a), while those in moderate El Niños are mostly confined to the central Pacific around 150°–170°W (Fig. 2c). Such a difference is consistent with the different warm patterns classified by the FCM (Figs. 1a,b). Moreover, the SSTA tendencies during the developing phase display similar zonal patterns to the corresponding SSTAs, with more positive values in the eastern (central) than in the central (eastern) equatorial Pacific in extreme (moderate) El Niños (Figs. 2b,d, contours). On the other hand, the damping effects of  $Q'_{net}$  in extreme and moderate El Niños are both larger in the eastern equatorial Pacific east of 140°W, albeit with a larger amplitude for the extreme ones (Figs. 2b,d). The former matches well with the corresponding gradual increases of positive SSTAs from the central to the eastern equatorial Pacific (Fig. 2e, solid curves), thus generally displaying a “larger warming gets more damping” zonal paradigm, while the latter zonally deviates from the corresponding larger positive SSTAs in the central equatorial Pacific west of 140°W (Fig. 2e, dashed curves). Accordingly, in moderate El Niños, the more damping effects of  $Q'_{net}$  and the weaker positive SSTA tendencies, both in the eastern equatorial Pacific, imply that the damping effect of  $Q'_{net}$  may help contribute to the local weaker SSTA tendencies, favoring larger SSTA tendencies as well as larger SSTAs being located in the central equatorial Pacific (Fig. 2d). Similar results can be found based on the  $Q'_{net}$  from the GODAS and NCEP–NCAR datasets (Fig. 3). In these two datasets, the larger damping effects of  $Q'_{net}$  in extreme El Niños generally match well with the larger SSTA tendencies (Figs. 3a,b), while those in moderate El Niños zonally deviate from the larger SSTA tendencies (Figs. 3c,d).

With regard to each individual El Niño event, it is shown that all the three extreme El Niños exhibit larger positive (negative) SSTAs ( $Q'_{net}$ ) in the eastern than central equatorial Pacific, and most of the moderate El Niños display larger positive SSTAs (negative  $Q'_{net}$ ) in the central (eastern) than eastern (central) equatorial Pacific, leading to the average of positive SSTAs (negative  $Q'_{net}$ ) in moderate El Niños being larger in the central (eastern) equatorial Pacific (Fig. 4). Note that the 1994/95 El Niño event is an outlier of moderate El Niño with larger

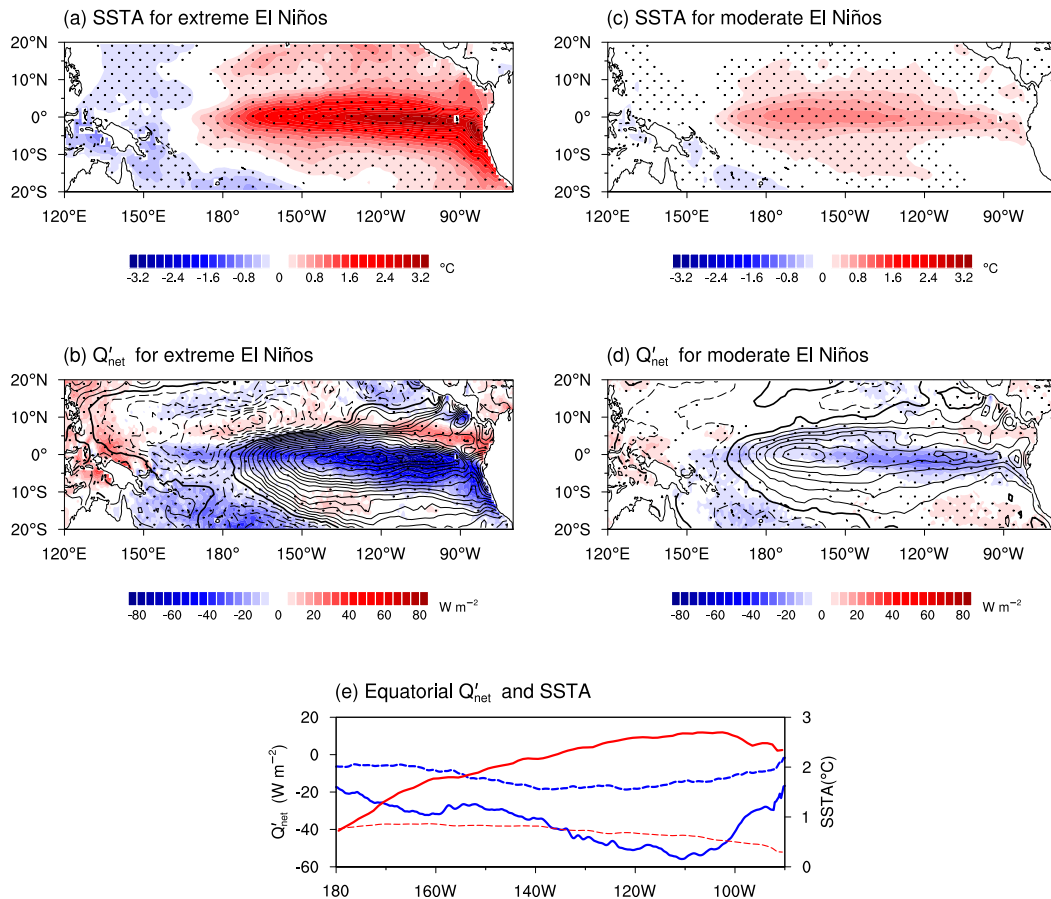


FIG. 2. Spatial patterns of (a) SSTAs and (b)  $Q'_{net}$  during the developing phase (May–December of the developing year) for extreme El Niños. Contours in (b) are the SSTA tendencies during the developing phase (units:  $^{\circ}\text{C month}^{-1}$ , with an interval of  $0.025^{\circ}\text{C month}^{-1}$ ; zero contour thickened and negative dashed). (c),(d) As in (a) and (b) but for moderate El Niños. Stippling indicates that the compositions of shaded values are significant at the 95% confidence level based on the Student's  $t$  test. (e) Zonal distributions of equatorial ( $2.5^{\circ}\text{S}$ – $2.5^{\circ}\text{N}$ )  $Q'_{net}$  (blue curves) and SSTA (red curves) for extreme (solid curves) and moderate (dashed curves) El Niños.

negative  $Q'_{net}$  in the central equatorial Pacific. In addition, there are slightly larger positive SSTAs but much larger negative  $Q'_{net}$  in the eastern equatorial Pacific for the 1987/88, 2009/10, and 2014/15 El Niño events. These outliers imply that there could be an intermediate state of SSTA pattern with no explicit difference between central and eastern Pacific warm anomalies (Chen et al. 2015). Nevertheless, they are classified into moderate El Niños as the zonal SSTA patterns of these three El Niños are closer to the second type based on the FCM (Fig. 1b). In the following section, we will reveal that the effects of  $Q'_{net}$  on the zonal SSTA pattern formations for these outliers are physically consistent with the common moderate El Niños.

Figure 5 displays a Hovmöller diagram (averaged over  $2.5^{\circ}\text{S}$ – $2.5^{\circ}\text{N}$ ) that compares the temporal evolutions of equatorial SSTAs as well as  $Q'_{net}$  during the developing year between extreme and moderate El Niño events. Extreme and moderate El Niños both present warm SSTAs first in the central equatorial Pacific in early spring of the developing year, and follow discrepant developing trajectories of the zonal

SSTA pattern afterward. In extreme El Niños, the largest SSTAs appear to be anchored basically in the eastern equatorial Pacific east of  $150^{\circ}\text{W}$  after May of the developing year (Fig. 5a), while those in moderate El Niños are mostly confined to the central Pacific around  $150^{\circ}$ – $170^{\circ}\text{W}$  (Fig. 5c). Such a difference is consistent with the different SSTA patterns averaged over the developing phase (Figs. 2a,c). Meanwhile, the SSTA tendencies during the developing phase show overall similar zonal distributions to the corresponding SSTAs, with more positive values in the eastern (central) than central (eastern) equatorial Pacific in extreme (moderate) El Niños (Figs. 5a,c, contours). On the other hand, the more damping effects of  $Q'_{net}$  in extreme and moderate El Niños are both located in the eastern equatorial Pacific during the developing phase (Figs. 5b,d). The former matches well with the corresponding zonal pattern of SSTAs, while the latter is anchored in the eastern equatorial Pacific and zonally deviates from the corresponding more positive SSTAs in the central equatorial Pacific.

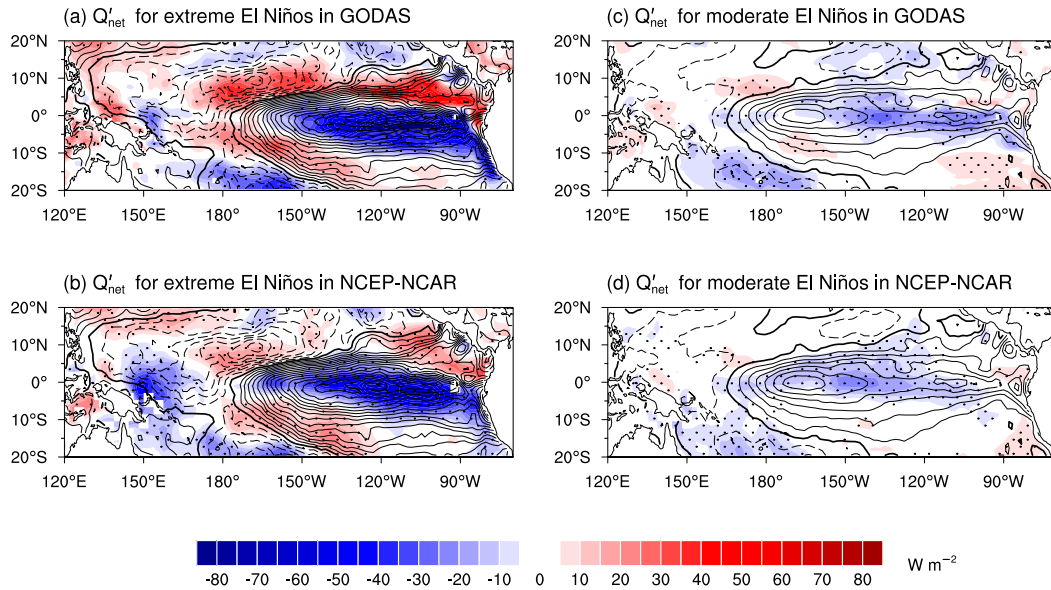


FIG. 3. As in Figs. 2b and 2d, but for  $Q'_{\text{net}}$  data from (a),(c) GODAS and (b),(d) NCEP-NCAR.

To quantify the discrepant effects of  $Q'_{\text{net}}$  on the development of zonal SSTa patterns between extreme and moderate El Niño, an ocean mixed layer heat budget analysis is further conducted based on the GODAS dataset (Fig. 6) during the

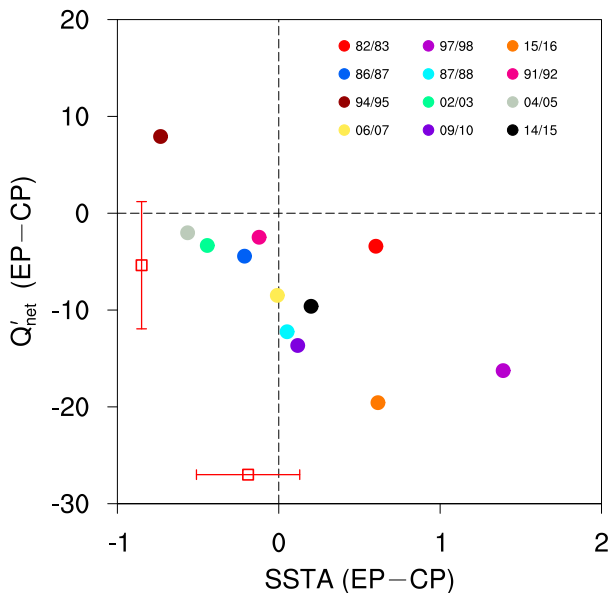


FIG. 4. Scatterplot of difference of SSTAs vs that of  $Q'_{\text{net}}$  between eastern Pacific ( $2.5^{\circ}\text{S}$ – $2.5^{\circ}\text{N}$ ,  $150^{\circ}$ – $90^{\circ}\text{W}$ ) and central Pacific ( $2.5^{\circ}\text{S}$ – $2.5^{\circ}\text{N}$ ,  $180^{\circ}$ – $150^{\circ}\text{W}$ ) for each individual El Niño event during the developing phase. The horizontal (vertical) red bar and the square box in the red bar denote the standard deviations and mean of SSTAs ( $Q'_{\text{net}}$ ) only for moderate El Niños, respectively. The standard deviations of SSTAs and  $Q'_{\text{net}}$  for moderate El Niños are indicated by red horizontal and vertical bars, respectively. The red square box in the horizontal (vertical) red bar denotes the mean of SSTAs ( $Q'_{\text{net}}$ ) for moderate El Niños.

developing phase of the two El Niño clusters both in the eastern ( $2.5^{\circ}\text{S}$ – $2.5^{\circ}\text{N}$ ,  $140^{\circ}$ – $90^{\circ}\text{W}$ ; red bars) and central equatorial Pacific ( $2.5^{\circ}\text{S}$ – $2.5^{\circ}\text{N}$ ,  $180^{\circ}$ – $140^{\circ}\text{W}$ ; blue bars), together with their differences (black bars). Note that the spatial patterns of the chosen mixed layer temperature anomalies are quite similar to those of the SSTAs both in extreme and moderate El Niños (not shown). Concurrent with the SSTA tendencies (Figs. 2b,d, contours), the ocean mixed layer temperature tendencies ( $C\partial T'_o/\partial t$ ) for extreme El Niños are larger in the eastern than central equatorial Pacific (Fig. 6a). Such zonal distribution is contributed by the ocean three-dimensional heat transport anomalies, among which the  $Q'_w$  contributes the most, consistent with previous studies (Kug et al. 2009; Chen et al. 2015). However,  $Q'_{\text{net}}$ , acting as the major damping term, displays a much more damping effect in the eastern than in the central equatorial Pacific. This indicates that the damping effect of  $Q'_{\text{net}}$  could not essentially alter the zonal distribution of  $C\partial T'_o/\partial t$  owing to the overwhelming positive effect from ocean heat transport anomalies; rather, it is merely a response to positive SSTAs.

By contrast, the  $C\partial T'_o/\partial t$  values in the central equatorial Pacific are a little bit larger than those in the eastern equatorial Pacific for moderate El Niños (Fig. 6b). Similar to the extreme El Niños, the contribution of ocean three-dimensional heat transport anomalies in moderate El Niños, albeit with a much smaller magnitude, also favors more positive SSTAs in the eastern than in the central Pacific, while the  $Q'_{\text{net}}$  acts to suppress such effect. This indicates that the more damping effects of  $Q'_{\text{net}}$  in the eastern equatorial Pacific might alter the zonal distribution of  $C\partial T'_o/\partial t$  in moderate El Niños by partly offsetting the local modest positive effects of ocean heat transport anomalies, favoring more positive SSTAs to be located in the central equatorial Pacific.

The  $Q'_{\text{res}}$  in extreme El Niños is negligible but appears to be another contributor to the zonal SSTA pattern formation in

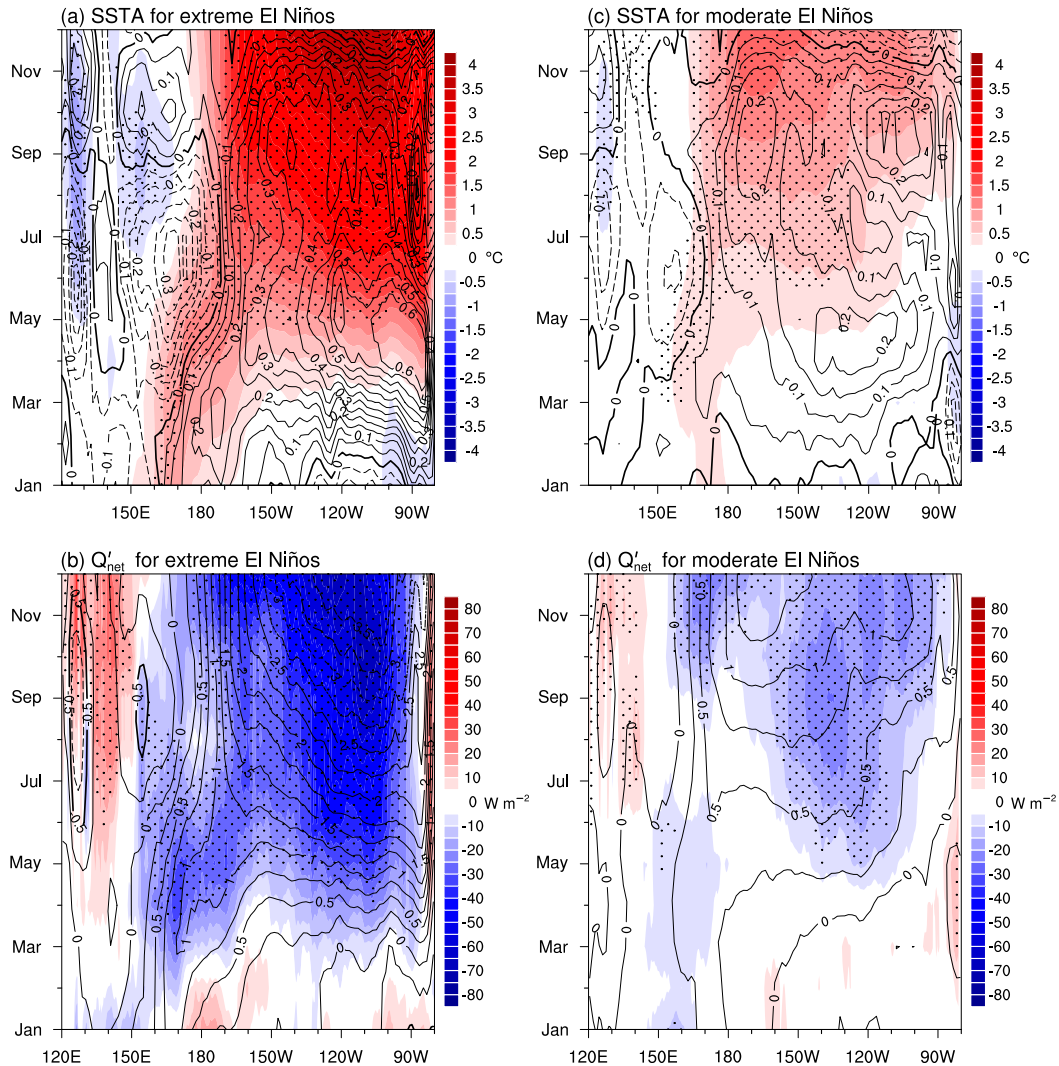


FIG. 5. Hovmöller diagram for equatorial (2.5°S–2.5°N) (a),(c) SSTAs and (b),(d) surface net heat flux anomalies during the developing year in (a),(b) extreme and (c),(d) moderate El Niños. Contours in (a) and (c) denote the tendency of SSTAs (units:  $^{\circ}C month^{-1}$ , with an interval of  $0.05^{\circ}C month^{-1}$ ; zero contour thickened and negative dashed), and in (b) and (d) denote the SSTAs (units:  $^{\circ}C$ , with an interval of  $0.25^{\circ}C$ ; zero contour thickened and negative dashed). Stippling indicates that the compositions of shaded values are significant at the 95% confidence level based on the Student's  $t$  test.

moderate El Niños by producing negative (positive) effects in the eastern (central) Pacific, favoring more positive SSTAs in the central equatorial Pacific. Thus, the role of oceanic subgrid-scale processes, which are beyond the scope of this study, should be paid more attention to in shaping the zonal SSTA pattern of moderate El Niños.

#### c. Discrepant atmospheric adjustments involved in $Q'_{net}$ between extreme and moderate El Niños

Figure 7 displays the spatial patterns of  $Q'_{SW}$ ,  $Q'_E$ , and the sum of both in the developing phase for the two types of El Niño. It is shown that the sum of  $Q'_E$  and  $Q'_{SW}$  matches well with the spatial patterns of  $Q'_{net}$ , both in extreme and moderate El Niños, with the spatial correlations both exceeding 0.98

(Figs. 7c,f). This indicates that the  $Q'_E$  and  $Q'_{SW}$  terms dominate  $Q'_{net}$ , while the  $Q'_H$  and  $Q'_{LW}$  terms (not shown) are negligible. The negative  $Q'_{SW}$ , with their damping centers being located in the central equatorial Pacific in response to the atmospheric deep convection anomalies, extend to the eastern equatorial Pacific in extreme El Niños (Fig. 7a), but are confined to the central equatorial Pacific west of 180° and the north of the eastern Pacific in moderate El Niños (Fig. 7d). The  $Q'_E$  exhibits a zonal dipole pattern both in extreme and moderate El Niños, with weak (strong) positive (negative) anomalies in the central (eastern) equatorial Pacific (Figs. 7b,e). The sum of  $Q'_{SW}$  and  $Q'_E$  shows that the positive effects of  $Q'_E$  in the central equatorial Pacific are totally offset by the local negative effects of  $Q'_{SW}$ , and the negative effects of  $Q'_E$  dominate the damping

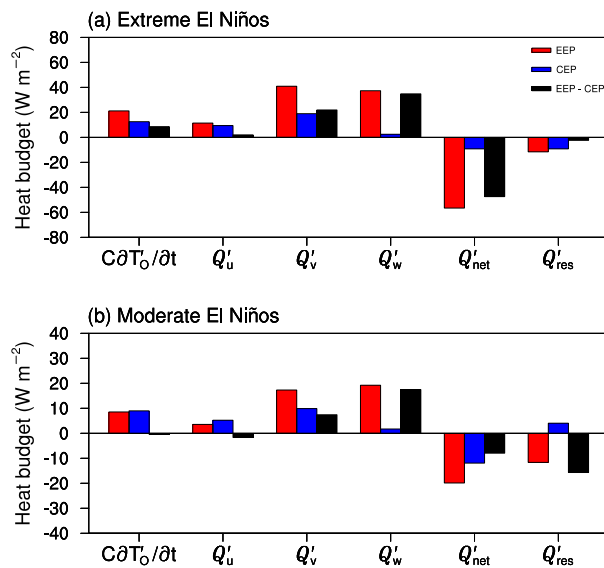


FIG. 6. The ocean mixed layer heat budget during the developing phase of (a) extreme and (b) moderate El Niños based on GODAS. The red, blue, and black bars denote the regional-mean values in the eastern equatorial Pacific (EEP;  $2.5^{\circ}\text{S}$ – $2.5^{\circ}\text{N}$ ,  $140^{\circ}$ – $90^{\circ}\text{W}$ ), the central equatorial Pacific (CEP;  $2.5^{\circ}\text{S}$ – $2.5^{\circ}\text{N}$ ,  $180^{\circ}$ – $140^{\circ}\text{W}$ ), and their differences (EEP minus CEP). The  $C\partial T'_0/\partial t$ ,  $Q'_u$ ,  $Q'_v$ ,  $Q'_w$ ,  $Q'_{\text{net}}$ , and  $Q'_{\text{res}}$  terms represent the tendency of mixed layer temperature anomalies, the mixed layer zonal, meridional and vertical heat transport anomalies, surface net heat flux anomalies, and residual term, respectively. Note that the values on the y axis are different between (a) and (b).

role of  $Q'_{\text{net}}$  in the eastern equatorial Pacific, leading to relatively weak damping effects in the central equatorial Pacific and strong damping effects in the eastern equatorial Pacific, both in extreme and moderate El Niños (Figs. 7c,f). Therefore, the  $Q'_E$  plays a dominant role both in the “larger warming gets more damping” zonal paradigm of  $Q'_{\text{net}}$  in extreme El Niños and in the zonal deviation between the positive SSTA center and the negative  $Q'_{\text{net}}$  center in moderate El Niños.

The factors contributing to  $Q'_E$  are further compared between extreme and moderate El Niños (Fig. 8). The reconstructed spatial patterns and magnitudes of  $Q'_E$  in extreme and moderate El Niños are almost identical compared with their original counterparts (Figs. 7b,e), with the spatial correlations both exceeding 0.97, indicating that the decomposition of  $Q'_E$  based on Eq. (6) is reasonable. The oceanic response represented by  $Q'_{\text{EO}}$  plays a negative role both in extreme and moderate El Niños (Figs. 8b,g). Regarding the atmospheric adjustments, the  $Q'_{\text{EW}}$  is totally negative in the eastern equatorial Pacific in moderate El Niños, but involves both positive and negative effects in extreme El Niños (Figs. 8c,h); the  $Q'_{\text{ERH}}$  term appears to play a critical role in the damping effects of  $Q'_E$  in the eastern equatorial Pacific both in extreme and moderate El Niños (Figs. 8d,i); and the  $Q'_{\text{EAT}}$  term plays another important role for the damping effects in the eastern equatorial Pacific in extreme El Niños with local robust positive SSTAs, but is negligible in moderate El Niños with weak SSTAs (Figs. 8e,j).

The discrepant effects of  $Q'_{\text{EW}}$  in the eastern equatorial Pacific between extreme and moderate El Niños could be due to local different positive WES feedback processes. In extreme El Niños, the robust positive SSTAs in the eastern equatorial Pacific trigger local deep convections (Fig. 7a, contours). The convective heating causes surface convergent anomalies in the eastern equatorial Pacific, including the intrusion of strong westerly wind anomalies from the central to the eastern equatorial Pacific (Fig. 9a; Xie et al. 2018) and the convergence of meridional wind anomalies to the equator (Fig. 9b). The intrusion of westerly anomalies weakens the background easterly winds and lowers the surface evaporation, contributing positively to the growth of warm SSTAs in the eastern equatorial Pacific (Fig. 9a), while the convergence of meridional wind anomalies weakens (enhances) the background cross-equatorial southerly winds and increases (decreases) the SSTAs north (south) of the equator (Fig. 9b). The positive and negative effects of  $Q'_{\text{EW}}$  largely counterbalance each other in the eastern equatorial Pacific, leading to relatively small negative effects on the growth of SSTAs (Fig. 8c). In moderate El Niños, however, the relatively weak positive SSTAs in the eastern Pacific cannot trigger local deep convections due to too cold background SST, but could be sufficient enough to trigger deep convections in the central equatorial Pacific and the climatological ITCZ region north of the eastern Pacific where the background SSTs are already high (Fig. 7d, contours), thus causing westerly anomalies confined to the central-western Pacific and cross-equatorial southeasterly anomalies in the eastern equatorial Pacific (Figs. 9c,d). The SSTA-induced southeasterly anomalies can feed back to the further development of SSTAs by enhancing the background southeasterlies and evaporation through the WES feedback, which produce prominent damping effects on the subsequent growth of SSTAs in the eastern equatorial Pacific and favor larger SSTAs to be located in the central equatorial Pacific.

The damping effects of  $Q'_{\text{ERH}}$  in the eastern equatorial Pacific could be attributable to the local negative feedback between SST and relative humidity. To verify such feedback, we define a relative humidity–SST feedback index (RSFI) by regressing the monthly anomalies of surface relative humidity onto the SSTAs. As shown in Fig. 10a, prominent negative RSFI values appear in the eastern equatorial Pacific. This indicates that the positive SSTAs in the eastern equatorial Pacific during El Niño events will reduce the local relative humidity, which further suppresses the growth of local SSTAs by inducing negative  $Q'_E$  (Figs. 8d,i). Such inherent negative feedback could be due to local strong vertical mixing between the boundary layer with relatively high relative humidity and the upper free atmosphere with relatively low relative humidity (Fig. 10c, contours) that is induced by positive SSTAs. The positive SSTAs increase the production of vertical mixing in the eastern Pacific boundary layer where the stratocumulus prevails (Wood 2012), thus enhancing the entrainment of upper-level dry air at the stratus cloud top, which tends to desiccate the whole boundary layer (Scott et al. 2020) and raise the boundary layer height. Indeed, the equatorial RSFIs are negative from the surface to the top of the boundary layer (which is also the stratus cloud top) where the climatological

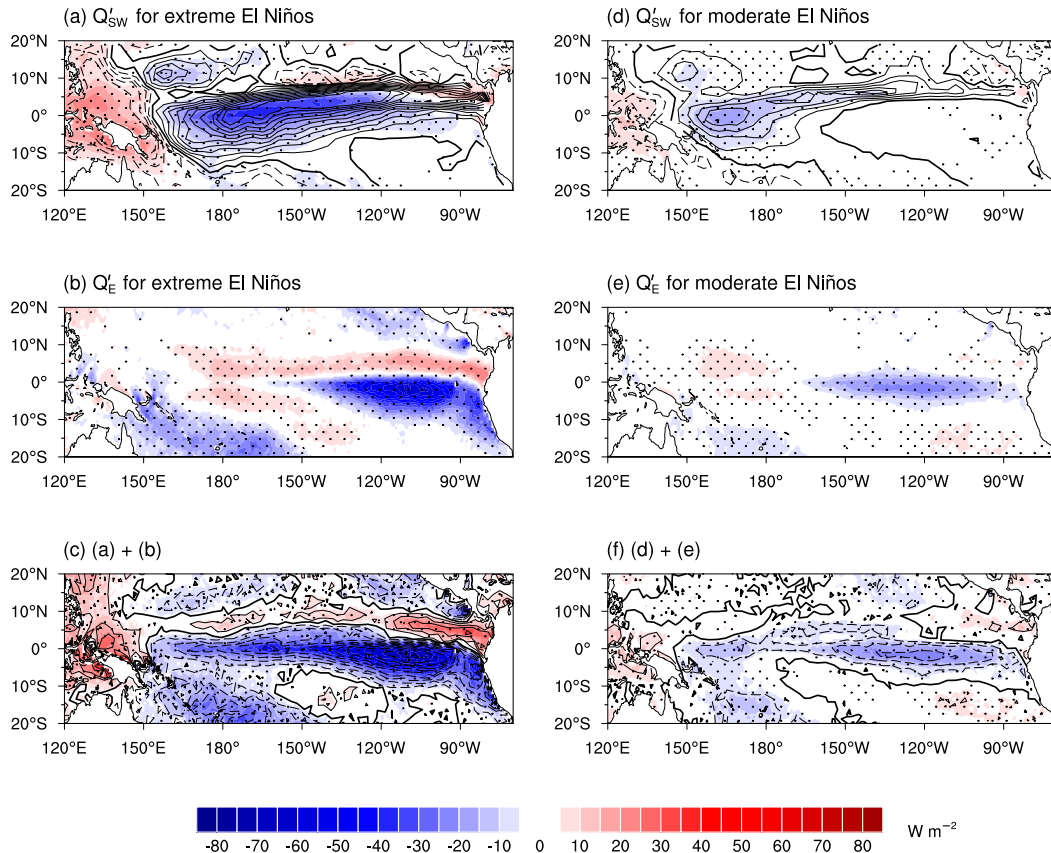


FIG. 7. Spatial patterns of (a) surface net shortwave radiation anomalies, (b) surface latent heat flux anomalies, and (c) the sum of the two in extreme El Niños. The black contours in (a) and (c) are the spatial patterns of precipitation anomalies (units:  $^{\circ}\text{C}$ , with an interval of  $0.5 \text{ mm day}^{-1}$ ; zero contour thickened and negative dashed) and surface net heat flux anomalies (units:  $\text{W m}^{-2}$ , with an interval of  $7.5 \text{ W m}^{-2}$ ; zero contour thickened and negative dashed), respectively. (d)–(f) As in (a)–(c), but for moderate El Niños. Stippling indicates that the compositions of shaded values are significant at the 95% confidence level based on the Student's  $t$  test.

relative humidity is the largest due to the vertical mixing, but are positive in the upper free atmosphere (Fig. 10c, shaded). Moreover, there are positive feedbacks between the monthly anomalies of boundary layer height and SST in the eastern equatorial Pacific (BHFI, Fig. 10b), further verifying a stronger vertical mixing between the boundary layer and the free atmosphere that helps to reduce the surface relative humidity during El Niño events (Deser and Wallace 1990; Ham et al. 2018). Therefore, no matter which type of El Niño occurs, the inherent negative relative humidity–SST feedback helps to confine the damping effects of  $Q'_E$  to the eastern equatorial Pacific, contributing to both the “larger warming gets more damping” zonal paradigm in extreme El Niños and the more SSTAs in the central equatorial Pacific in moderate El Niños.

Figure 11 quantifies the major flux anomalies during the developing phase of El Niño both in the eastern ( $2.5^{\circ}\text{S}$ – $2.5^{\circ}\text{N}$ ,  $140^{\circ}$ – $90^{\circ}\text{W}$ ) and central ( $2.5^{\circ}\text{S}$ – $2.5^{\circ}\text{N}$ ,  $180^{\circ}$ – $140^{\circ}\text{W}$ ) equatorial Pacific, as well as their differences. In extreme El Niños with the larger SSTAs in the eastern equatorial Pacific,  $Q'_{\text{net}}$  is mainly contributed by both  $Q'_{\text{SW}}$  and  $Q'_E$ . The former contributes more damping effects in the central equatorial Pacific,

which are partly offset by the local positive effects of  $Q'_{\text{EW}}$  involved in  $Q'_E$ , while the latter plays a dominant damping role in the eastern equatorial Pacific, which is mainly contributed by  $Q'_{\text{EO}}$ ,  $Q'_{\text{ERH}}$ , and  $Q'_{\text{EAT}}$ . In moderate El Niños with the larger SSTAs in the central equatorial Pacific, the zonal deviation between the positive SSTA center and the negative  $Q'_{\text{net}}$  center is mainly caused by more damping effects of  $Q'_E$  in the eastern equatorial Pacific, which are mainly contributed by  $Q'_{\text{EO}}$ ,  $Q'_{\text{EW}}$ , and  $Q'_{\text{ERH}}$ . Thus, apart from the oceanic response ( $Q'_{\text{EO}}$ ), it appears that the positive WES feedback and the negative relative humidity–SST feedback in the eastern equatorial Pacific are the two major atmospheric adjustments that lead to the zonal deviation between the positive SSTA center in the central Pacific and the negative  $Q'_{\text{net}}$  center in the eastern Pacific, favoring the largest SSTAs being confined to the central equatorial Pacific in moderate El Niños.

#### 4. Conclusions and discussion

In this study, we reveal that the surface net heat flux anomalies ( $Q'_{\text{net}}$ ), once commonly regarded as responses to SSTAs in

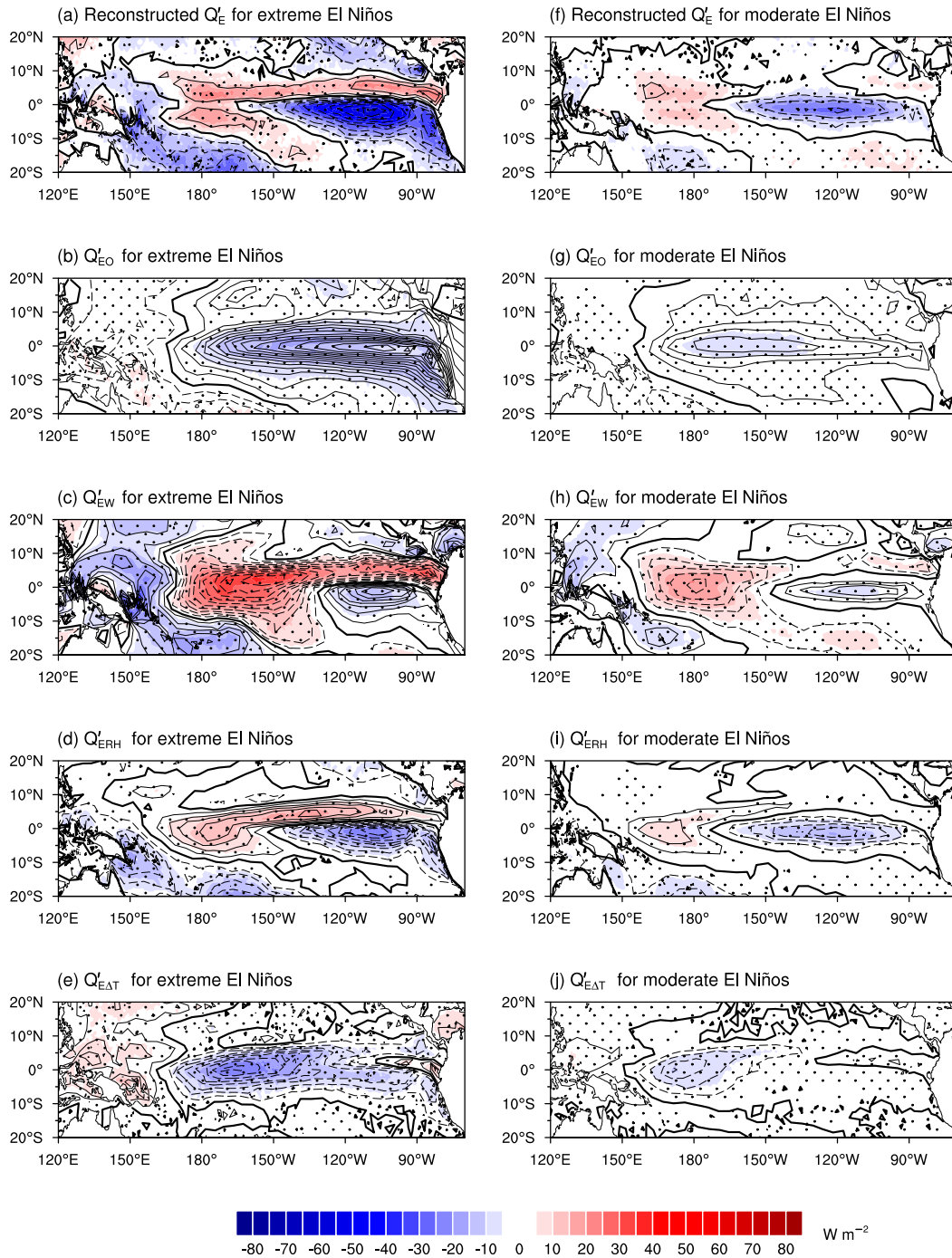


FIG. 8. Spatial patterns of the (a) reconstructed surface latent heat flux anomalies based on Eq. (6) and (b)–(e) each factor involved in the surface latent heat flux anomalies in extreme El Niños based on Eqs. (7)–(10): (b) the Newtonian cooling effect, and the atmospheric forcing effect due to anomalies in (c) surface wind speed, (d) relative humidity, and (e) surface stability. Contours in (a)–(e) are the spatial patterns of the original surface latent heat flux anomalies (units:  $\text{W m}^{-2}$ , with an interval of  $7.5 \text{ W m}^{-2}$ ; zero contour thickened and negative dashed), the SSTAs (units:  $^{\circ}\text{C}$ , with an interval of  $0.2^{\circ}\text{C}$ ; zero contour thickened and negative dashed), the surface wind speed anomalies (units:  $\text{m s}^{-1}$ , with an interval of  $0.15 \text{ m s}^{-1}$ ; zero contour thickened and negative dashed), the relative humidity anomalies (with an interval of  $7.5 \times 10^{-3}$ ; zero contour thickened and negative dashed), and the surface stability anomalies (units:  $^{\circ}\text{C}$ , with an interval of  $0.15^{\circ}\text{C}$ ; zero contour thickened and negative dashed), respectively. (f)–(j) As in (a)–(e), but for moderate El Niños. Stippling indicates that the compositions of shaded values are significant at the 95% confidence level based on the Student's  $t$  test.

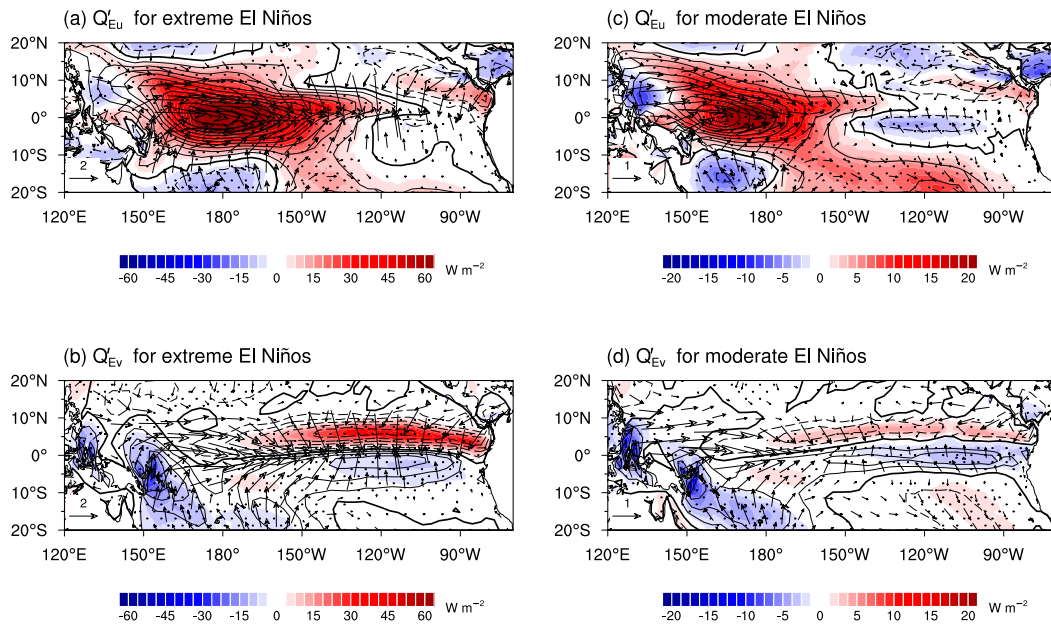


FIG. 9. Spatial patterns of the atmospheric forcing effect due to anomalies in (a) surface zonal wind speed and (b) meridional wind speed in extreme El Niños. Contours in (a) and (b) are the surface zonal wind anomalies and meridional wind anomalies (units:  $\text{m s}^{-1}$ , with an interval of  $0.4 \text{ m s}^{-1}$ ; zero contour thickened and negative dashed), respectively. Vectors in (a) and (b) are the surface wind vector anomalies (units:  $\text{m s}^{-1}$ ). (c),(d) As in (a) and (b), but for moderate El Niños. Note that the interval of contours in (c) and (d) is  $0.2 \text{ m s}^{-1}$ , which is different from that in (a) and (b). Stippling indicates that the compositions of shaded values are significant at the 95% confidence level based on the Student's  $t$  test.

El Niño events, can play different roles in the formation of SSTA patterns in different El Niño types. By applying the FCM, the El Niño events during the period 1982–2018 are classified into two types: extreme El Niños and moderate El Niños. The former displays robust positive SSTAs and has its largest SSTAs in the eastern equatorial Pacific, while the latter exhibits relatively weak positive SSTAs and has its largest SSTAs in the central equatorial Pacific. It is shown that the damping effects of  $Q'_{\text{net}}$  in the developing phase of extreme and moderate El Niños are both larger in the eastern than in the central equatorial Pacific. The former generally displays a “larger warming gets more damping” zonal paradigm and essentially does not impact the spatial pattern of SSTA tendencies as well as the pattern formation of SSTAs, while the latter can impact the spatial pattern formation of SSTAs by damping the SSTA tendencies more in the eastern than in the central equatorial Pacific, favoring the positive center of SSTAs being confined to the central equatorial Pacific. An ocean mixed layer heat budget analysis indicates that the merely damping role of  $Q'_{\text{net}}$  in extreme El Niños could be attributable to the overwhelming modulation of ocean heat transport anomalies, which play a decisive role in the spatial pattern formation of SSTAs. Meanwhile, the  $Q'_{\text{net}}$  in moderate El Niños could be a contributor to the SSTA pattern formation largely owing to the modest modulation of ocean heat transport anomalies, leaving room for the damping effects of  $Q'_{\text{net}}$  to function.

The  $Q'_{\text{net}}$  term is mainly contributed by surface net shortwave radiation anomalies and surface latent heat flux anomalies ( $Q'_E$ ), both in extreme and moderate El Niños, among which

the latter plays a dominant role. However, the atmospheric adjustments involved in  $Q'_E$  play out differently between extreme and moderate El Niños. In extreme El Niños, the negative relative humidity–SST feedback and the reduced surface stability due to robust SSTAs are the two major atmospheric adjustments for the damping effects of  $Q'_E$  in the eastern equatorial Pacific, while the WES feedback plays a negligible role owing to the counterbalance between the positive effects from the eastward intrusion of the westerlies and the negative effects from the equatorial convergence of meridional wind anomalies.

In moderate El Niños, the negative relative humidity–SST feedback also appears to be the most dominant atmospheric adjustments for the damping effects of  $Q'_E$  in the eastern equatorial Pacific, suggesting that the negative relative humidity–SST feedback is an inherent regulator that helps to confine the damping effects of  $Q'_E$  to the eastern equatorial Pacific regardless of the type of El Niño. In addition, the WES feedback is revealed to be another major atmospheric adjustment for the damping effects of  $Q'_E$  in the eastern equatorial Pacific, which is a result of local cross-equatorial southeasterly anomalies caused by SSTA-induced deep convection anomalies north of the eastern Pacific. Previous studies have revealed that the effects of eastern Pacific wind anomalies are crucial for the discrepant decay trajectories between extreme and moderate El Niño through different ocean dynamical heat transports and WES feedback (Xie et al. 2018; Peng et al. 2020). Here we highlight that the different wind anomalies during the developing phase also play roles in the formation of different SSTA patterns between extreme and

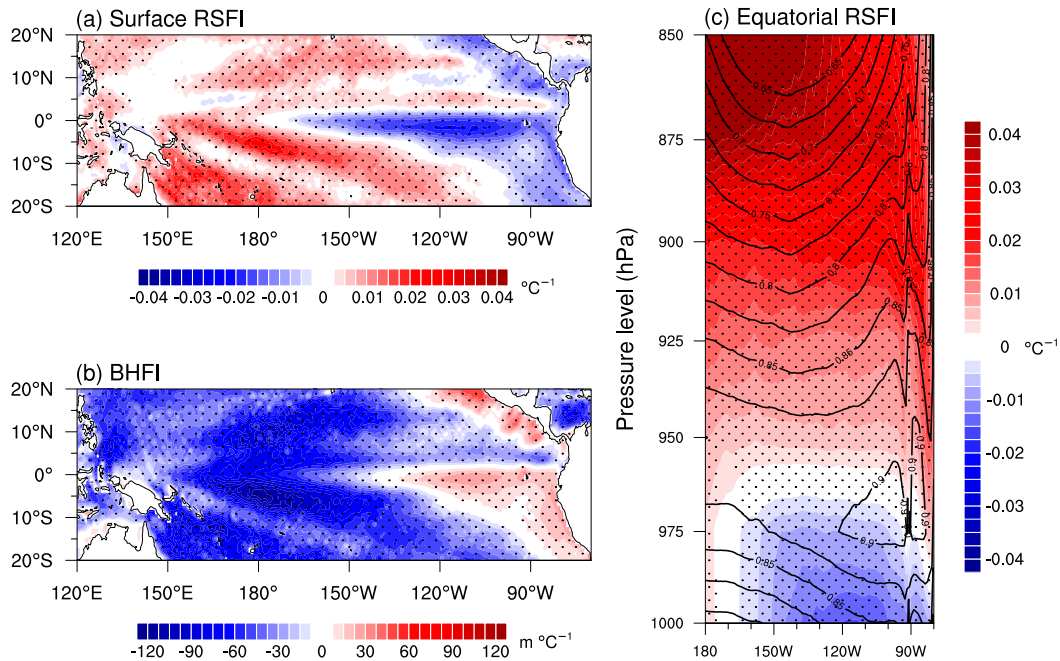


FIG. 10. Spatial patterns of (a) relative humidity–SST feedback index (RSFI) and (b) boundary layer height–SST feedback index (BHFI). (c) Vertical distribution of equatorial (2.5°S–2.5°N) RSFI in the eastern Pacific. Contours in (c) denote the climatological relative humidity. Stippling indicates that the regressions are significant at the 95% confidence level based on the Student's  $t$  test.

moderate El Niño owing to the emergence of different SSTA-induced convective anomalies (Figs. 7a,d, contours). Therefore, it is mainly the two atmospheric adjustments, the negative relative humidity–SST feedback and the positive WES feedback, that favor the damping effects of  $Q_{\text{net}}$  to be more in the eastern than in the central equatorial Pacific and contribute to more positive SSTAs in the central equatorial Pacific in moderate El Niños. The former plays a dominant role, while the latter plays a secondary role.

The classification of El Niño diversity has been always a heated debate in climate research community (Kao and Yu 2009; Takahashi et al. 2011; Karnauskas 2013; Chen et al. 2015). In a pioneering application of the FCM to the classification of El Niño by Chen et al. (2015), three warm patterns are classified—the extreme El Niños, which are identical to the current first warm pattern; the warm-pool El Niños, which has weak positive SSTAs centered near the date line; and the canonical El Niños with moderate positive SSTAs along the central-eastern equatorial Pacific. In this study, however, we do not try to clarify different types of El Niño, but to explore different atmospheric adjustments specifically between extreme and other nonextreme El Niños. Therefore, the number of cluster set chosen here is two [i.e.,  $M = 2$  in (1)] to highlight the different warm patterns between extreme El Niños and other moderate ones. The main conclusions in this study do not change essentially between the extreme El Niños and the other two nonextreme El Niños if three types of El Niño are classified as in Chen et al. (2015).

The present study focuses on the discrepant effects of atmospheric adjustments on the formation of zonal SSTA patterns in different El Niño types, with a particular focus on

contributions of atmospheric adjustments in the formation of SSTA patterns in moderate El Niños, while the effects of ocean heat transport anomalies have not been explored extensively. In fact, many studies have revealed that some specific ocean dynamical processes play key roles in the development of SSTAs in specific El Niño types (Kug et al. 2009; Chen et al. 2015; Lian et al. 2017). For instance, ocean thermocline feedback was revealed to play the dominant role in the development of extreme El Niños (Chen et al. 2015), while zonal advective feedback plays a crucial role during warm pool El Niños (which essentially can be classified into moderate El Niños in the current study) (Kug et al. 2009; Takahashi et al. 2011). Thus, the atmospheric adjustment processes, especially for the relative humidity–SST feedback and the WES feedback in the eastern equatorial Pacific, could be supplementary mechanisms in modulating the zonal pattern formation of SSTAs in moderate El Niños, and do not conflict with previous ocean origin mechanisms. Moreover, these atmospheric adjustments may play potential roles in predicting the SSTA pattern of El Niño during the peak phase. For example, if the SSTA-induced deep convections do not move to the eastern Pacific to trigger the conventional Bjerknes feedback during the developing phase of an El Niño (Karnauskas 2013; Lian et al. 2017), the positive SSTA center in the peak phase is likely to be closer to the central equatorial Pacific, as the damping effects from atmospheric adjustments will further suppress the growth of SSTAs in the eastern equatorial Pacific. They may also explain, to some extent, why there are only few cases that have the spatial patterns similar to extreme El Niño but with their magnitudes similar to moderate El Niño (McPhaden et al. 2011; Zhang et al. 2015), although more

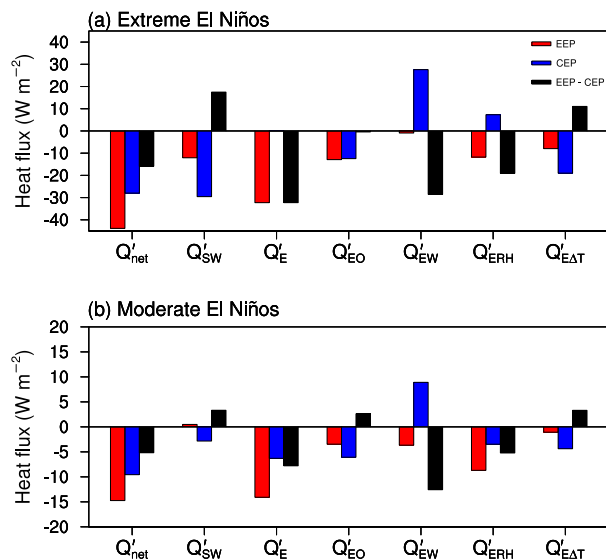


FIG. 11. The major heat flux anomalies during the developing phase of (a) extreme and (b) moderate El Niños. The red, blue, and black bars denote the regional-mean values in the eastern equatorial Pacific ( $2.5^{\circ}\text{S}$ – $2.5^{\circ}\text{N}$ ,  $140^{\circ}$ – $90^{\circ}\text{W}$ ), the central equatorial Pacific ( $2.5^{\circ}\text{S}$ – $2.5^{\circ}\text{N}$ ,  $180^{\circ}$ – $140^{\circ}\text{W}$ ), and their differences (eastern Pacific minus central Pacific). The  $Q'_{\text{net}}$ ,  $Q'_{\text{SW}}$ ,  $Q'_E$ ,  $Q'_{\text{EO}}$ ,  $Q'_{\text{EW}}$ ,  $Q'_{\text{ERH}}$ , and  $Q'_{\text{EAT}}$  terms denote the surface net heat flux anomalies, the surface net shortwave radiation anomalies, the surface latent heat flux anomalies, the Newtonian cooling effect, and the atmospheric adjustments due to anomalies in surface wind speed, relative humidity, and surface stability, respectively. Note that the values on the y axis are different between (a) and (b).

details need to be provided to verify such interpretation. We highlight that atmospheric adjustments should be considered during the development of moderate El Niños in order to obtain a comprehensive understanding of the formation of El Niño diversity.

**Acknowledgments.** This work was supported by the Scientific Research Fund of the Second Institute of Oceanography, Ministry of Natural Resources (Grant QNYC2001), the National Natural Science Foundation of China (Grants 41690121, 41690120, 41706024, 41621064, 41831175), the Indo-Pacific Ocean Variability and Air–Sea Interaction (IPOVAI; Grant GASI-01-WPAC-STspr), the Youth Innovation Promotion Association of the Chinese Academy of Sciences, and the Key Deployment Project of Centre for Ocean Mega-Research of Science, Chinese Academy of Sciences (Grant COMS2019Q03). We thank Prof. Jian Ma and Dr. Qun Liu for their helpful discussions.

## REFERENCES

Alexander, M. A., I. Bladé, M. Newman, J. R. Lanzante, N.-C. Lau, and J. D. Scott, 2002: The atmospheric bridge: The influence of ENSO teleconnections on air–sea interaction over the global oceans. *J. Climate*, **15**, 2205–2231, [https://doi.org/10.1175/1520-0442\(2002\)015<2205:TABTIO>2.0.CO;2](https://doi.org/10.1175/1520-0442(2002)015<2205:TABTIO>2.0.CO;2).

An, S.-I., J. S. Kug, A. Timmermann, I.-S. Kang, and O. Timm, 2007: The influence of ENSO on the generation of decadal variability in the North Pacific. *J. Climate*, **20**, 667–680, <https://doi.org/10.1175/JCLI4017.1>.

Ashok, K., S. K. Behera, S. A. Rao, H. Weng, and T. Yamagata, 2007: El Niño Modoki and its possible teleconnection. *J. Geophys. Res.*, **112**, C11007, <https://doi.org/10.1029/2006JC003798>.

Barsugli, J. J., J. S. Whitaker, A. F. Loughe, P. D. Sardeshmukh, and Z. Toth, 1999: The effect of the 1997/98 El Niño on individual large-scale weather events. *Bull. Amer. Meteor. Soc.*, **80**, 1399–1412, [https://doi.org/10.1175/1520-0477\(1999\)080<1399:TEOTEN>2.0.CO;2](https://doi.org/10.1175/1520-0477(1999)080<1399:TEOTEN>2.0.CO;2).

Bjerknes, J., 1969: Atmospheric teleconnections from the equatorial Pacific. *Mon. Wea. Rev.*, **97**, 163–172, [https://doi.org/10.1175/1520-0493\(1969\)097<0163:ATFTEP>2.3.CO;2](https://doi.org/10.1175/1520-0493(1969)097<0163:ATFTEP>2.3.CO;2).

Cai, W., and Coauthors, 2014: Increasing frequency of extreme El Niño events due to greenhouse warming. *Nat. Climate Change*, **4**, 111–116, <https://doi.org/10.1038/nclimate2100>.

—, and Coauthors, 2015: ENSO and greenhouse warming. *Nat. Climate Change*, **5**, 849–859, <https://doi.org/10.1038/nclimate2743>.

—, G. Wang, A. Santoso, X. Lin, and L. Wu, 2017: Definition of extreme El Niño and its impact on projected increase in extreme El Niño frequency. *Geophys. Res. Lett.*, **44**, 11 184–11 190, <https://doi.org/10.1002/2017GL075635>.

Capotondi, A., and Coauthors, 2015: Understanding ENSO diversity. *Bull. Amer. Meteor. Soc.*, **96**, 921–938, <https://doi.org/10.1175/BAMS-D-13-00117.1>.

Chen, D., and Coauthors, 2015: Strong influence of westerly wind bursts on El Niño diversity. *Nat. Geosci.*, **8**, 339–345, <https://doi.org/10.1038/ngeo2399>.

Chen, L., T. Li, S. K. Behera, and T. Doi, 2016: Distinctive precursory air–sea signals between regular and super El Niños. *Adv. Atmos. Sci.*, **33**, 996–1004, <https://doi.org/10.1007/s00376-016-5250-8>.

Deser, C., and J. M. Wallace, 1990: Large-scale atmospheric circulation features of warm and cold episodes in the tropical Pacific. *J. Climate*, **3**, 1254–1281, [https://doi.org/10.1175/1520-0442\(1990\)003<1254:LSACFO>2.0.CO;2](https://doi.org/10.1175/1520-0442(1990)003<1254:LSACFO>2.0.CO;2).

DiNezio, P. N., A. C. Clement, G. A. Vecchi, B. J. Soden, B. P. Kirtman, and S.-K. Lee, 2009: Climate response of the equatorial Pacific to global warming. *J. Climate*, **22**, 4873–4892, <https://doi.org/10.1175/2009JCLI2982.1>.

Du, Y., and S.-P. Xie, 2008: Role of atmospheric adjustments in the tropical Indian Ocean warming during the 20th century in climate models. *Geophys. Res. Lett.*, **35**, L08712, <https://doi.org/10.1029/2008GL033631>.

Feng, J., T. Lian, J. Ying, J. Li, and G. Li, 2020: Do CMIP5 models show El Niño diversity? *J. Climate*, **33**, 1619–1641, <https://doi.org/10.1175/JCLI-D-18-0854.1>.

Ham, Y.-G., J.-S. Kug, J.-Y. Choi, F.-F. Jin, and M. Watanabe, 2018: Inverse relationship between present-day tropical precipitation and its sensitivity to greenhouse warming. *Nat. Climate Change*, **8**, 64–69, <https://doi.org/10.1038/s41558-017-0033-5>.

Horel, J. D., and J. M. Wallace, 1981: Planetary-scale atmospheric phenomena associated with the Southern Oscillation. *Mon. Wea. Rev.*, **109**, 813–829, [https://doi.org/10.1175/1520-0493\(1981\)109<0813:PSAPAW>2.0.CO;2](https://doi.org/10.1175/1520-0493(1981)109<0813:PSAPAW>2.0.CO;2).

Hu, S., and A. V. Fedorov, 2018: Cross-equatorial winds control El Niño diversity and change. *Nat. Climate Change*, **8**, 798–802, <https://doi.org/10.1038/s41558-018-0248-0>.

Jia, F., and L. Wu, 2013: A study of response of the equatorial Pacific SST to doubled- $\text{CO}_2$  forcing in the coupled CAM-1.5-layer reduced-gravity ocean model. *J. Phys. Oceanogr.*, **43**, 1288–1300, <https://doi.org/10.1175/JPO-D-12-0144.1>.

- Jin, F.-F., S.-I. An, A. Timmermann, and J. Zhao, 2003: Strong El Niño events and nonlinear dynamical heating. *Geophys. Res. Lett.*, **30**, 1120, <https://doi.org/10.1029/2002GL016356>.
- , S. T. Kim, and L. Bejarano, 2006: A coupled-stability index for ENSO. *Geophys. Res. Lett.*, **33**, L23708, <https://doi.org/10.1029/2006GL027221>.
- Kao, H.-Y., and J.-Y. Yu, 2009: Contrasting eastern-Pacific and central-Pacific types of ENSO. *J. Climate*, **22**, 615–632, <https://doi.org/10.1175/2008JCLI2309.1>.
- Karnauskas, K. B., 2013: Can we distinguish canonical El Niño from Modoki? *Geophys. Res. Lett.*, **40**, 5246–5251, <https://doi.org/10.1002/grl.51007>.
- Kim, H.-M., P. Webster, and J. Curry, 2009: Impact of shifting patterns of Pacific Ocean warming on North Atlantic tropical cyclones. *Science*, **325**, 77–80, <https://doi.org/10.1126/science.1174062>.
- Kim, H.-S., J.-H. Kim, C.-H. Ho, and P.-S. Chu, 2011: Pattern classification of typhoon tracks using the fuzzy *c*-means clustering method. *J. Climate*, **24**, 488–508, <https://doi.org/10.1175/2010JCLI3751.1>.
- Kug, J.-S., F.-F. Jin, and S.-I. An, 2009: Two types of El Niño events: Cold tongue El Niño and warm pool El Niño. *J. Climate*, **22**, 1499–1515, <https://doi.org/10.1175/2008JCLI2624.1>.
- Larkin, N. K., and D. E. Harrison, 2005: On the definition of El Niño and associated seasonal average U.S. weather anomalies. *Geophys. Res. Lett.*, **32**, L13705, <https://doi.org/10.1029/2005GL022738>.
- Lengaigne, M., and G. A. Vecchi, 2010: Contrasting the termination of moderate and extreme El Niño events in coupled general circulation models. *Climate Dyn.*, **35**, 299–313, <https://doi.org/10.1007/s00382-009-0562-3>.
- Lian, T., D. Chen, and Y. Tang, 2017: Genesis of the 2014–2016 El Niño events. *Sci. China Earth Sci.*, **60**, 1589–1600, <https://doi.org/10.1007/s11430-016-8315-5>.
- McPhaden, M. J., S. E. Zebiak, and M. H. Glantz, 2006: ENSO as an integrating concept in Earth science. *Science*, **314**, 1740–1745, <https://doi.org/10.1126/science.1132588>.
- , T. Lee, and D. McClurg, 2011: El Niño and its relationship to changing background conditions in the tropical Pacific Ocean. *Geophys. Res. Lett.*, **38**, L15709, <https://doi.org/10.1029/2011GL048275>.
- Pavlakakis, K. G., N. Hatzianastassiou, C. Matsoukas, A. Fotiadi, and I. Vardavas, 2008: ENSO surface shortwave radiation forcing over the tropical Pacific. *Atmos. Chem. Phys.*, **8**, 5565–5577, <https://doi.org/10.5194/acp-8-5565-2008>.
- Peng, Q., S.-P. Xie, D. Wang, Y. Kamae, H. Zhang, S. Hu, X.-T. Zheng, and W. Wang, 2020: Eastern Pacific wind effect on the evolution of El Niño: Implications for ENSO diversity. *J. Climate*, **33**, 3197–3212, <https://doi.org/10.1175/JCLI-D-19-0435.1>.
- Pinker, R. T., S. A. Grodsky, B. Zhang, A. J. Busalacchi, and W.-Y. Chen, 2017: ENSO impact on surface radiative fluxes as observed from space. *J. Geophys. Res. Oceans*, **122**, 7880–7896, <https://doi.org/10.1002/2017JC012900>.
- Scott, R. C., T. A. Myers, J. R. Norris, M. D. Zelinka, S. A. Klein, M. Sun, and D. R. Doelling, 2020: Observed sensitivity of low-cloud radiative effects to meteorological perturbations over the global oceans. *J. Climate*, **33**, 7717–7734, <https://doi.org/10.1175/JCLI-D-19-1028.1>.
- Takahashi, K., A. Montecinos, K. Goubanova, and B. Dewitte, 2011: ENSO regimes: Reinterpreting the canonical and Modoki El Niño. *Geophys. Res. Lett.*, **38**, L10704, <https://doi.org/10.1029/2011GL047364>.
- Taschetto, A. S., and M. H. England, 2009: El Niño Modoki impacts on Australian rainfall. *J. Climate*, **22**, 3167–3174, <https://doi.org/10.1175/2008JCLI2589.1>.
- , R. R. Rodrigues, G. A. Meehl, S. McGregor, and M. H. England, 2016: How sensitive are the Pacific–tropical North Atlantic teleconnections to the position and intensity of El Niño–related warming? *Climate Dyn.*, **46**, 1841–1860, <https://doi.org/10.1007/s00382-015-2679-x>.
- Timmermann, A., and Coauthors, 2018: El Niño–Southern Oscillation complexity. *Nature*, **559**, 535–545, <https://doi.org/10.1038/s41586-018-0252-6>.
- Tziperman, E., M. A. Cane, S. E. Zebiak, Y. Xue, and B. Blumenthal, 1998: Locking of El Niño’s peak time to the end of the calendar year in the delayed oscillator picture of ENSO. *J. Climate*, **11**, 2191–2199, [https://doi.org/10.1175/1520-0442\(1998\)011<2191:LOENOS>2.0.CO;2](https://doi.org/10.1175/1520-0442(1998)011<2191:LOENOS>2.0.CO;2).
- Wang, W., and M. J. McPhaden, 2000: The surface-layer heat balance in the equatorial Pacific Ocean. Part II: Interannual variability. *J. Phys. Oceanogr.*, **30**, 2989–3008, [https://doi.org/10.1175/1520-0485\(2001\)031<2989:TSLHBI>2.0.CO;2](https://doi.org/10.1175/1520-0485(2001)031<2989:TSLHBI>2.0.CO;2).
- Wei, K., C. Ouyang, H. Duan, Y. Li, M. Chen, J. Ma, H. An, and S. Zhou, 2020: Reflections on the catastrophic 2020 Yangtze River Basin flooding in southern China. *Innovation*, **1**, 100038, <https://doi.org/10.1016/j.xinn.2020.100038>.
- Wood, R., 2012: Stratocumulus clouds. *Mon. Wea. Rev.*, **140**, 2373–2423, <https://doi.org/10.1175/MWR-D-11-00121.1>.
- Wu, M. C., W. L. Chang, and W. M. Leung, 2004: Impacts of El Niño–southern oscillation events on tropical cyclone landfalling activity in the western North Pacific. *J. Climate*, **17**, 1419–1428, [https://doi.org/10.1175/1520-0442\(2004\)017<1419:IOENOE>2.0.CO;2](https://doi.org/10.1175/1520-0442(2004)017<1419:IOENOE>2.0.CO;2).
- Xie, S.-P., and S. G. H. Philander, 1994: A coupled ocean–atmosphere model of relevance to the ITCZ in the eastern Pacific. *Tellus*, **46**, 340–350, <https://doi.org/10.3402/tellusa.v46i4.15484>.
- , C. Deser, G. A. Vecchi, J. Ma, H. Teng, and A. T. Wittenberg, 2010: Global warming pattern formation: Sea surface temperature and rainfall. *J. Climate*, **23**, 966–986, <https://doi.org/10.1175/2009JCLI3329.1>.
- , Q. Peng, Y. Kamae, X.-T. Zheng, H. Tokinaga, and D. Wang, 2018: Eastern Pacific ITCZ dipole and ENSO diversity. *J. Climate*, **31**, 4449–4462, <https://doi.org/10.1175/JCLI-D-17-0905.1>.
- Xu, K., Q.-L. Huang, C.-Y. Tam, W. Wang, S. Chen, and C. Zhu, 2019: Roles of tropical SST patterns during two types of ENSO in modulating wintertime rainfall over southern China. *Climate Dyn.*, **52**, 523–538, <https://doi.org/10.1007/s00382-018-4170-y>.
- Yang, X., and P. Huang, 2021: Restored relationship between ENSO and Indian summer monsoon rainfall around 1999/2000. *Innovation*, **2**, 100102, <https://doi.org/10.1016/j.xinn.2021.100102>.
- Ying, J., P. Huang, and R. Huang, 2016: Evaluating the formation mechanisms of the equatorial Pacific SST warming pattern in CMIP5 models. *Adv. Atmos. Sci.*, **33**, 433–441, <https://doi.org/10.1007/s00376-015-5184-6>.
- Yuan, Y., and S. Yang, 2012: Impacts of different types of El Niño on the East Asian climate: Focus on ENSO cycles. *J. Climate*, **25**, 7702–7722, <https://doi.org/10.1175/JCLI-D-11-00576.1>.
- Zhang, W., H. Li, F.-F. Jin, M. F. Stuecker, A. G. Turner, and N. P. Klingaman, 2015: The annual-cycle modulation of meridional asymmetry in ENSO’s atmospheric response and its dependence on ENSO zonal structure. *J. Climate*, **28**, 5795–5812, <https://doi.org/10.1175/JCLI-D-14-00724.1>.
- Zhang, X., and M. J. McPhaden, 2008: Eastern equatorial Pacific forcing of ENSO sea surface temperature anomalies. *J. Climate*, **21**, 6070–6079, <https://doi.org/10.1175/2008JCLI2422.1>.